Inertial-Acoustic Oscillations of Black-Hole Accretion Discs with Large-Scale Poloidal Magnetic Fields

Cong Yu[1,2,3]*, and Dong Lai[2]
[1] *Yunnan Observatories, Chinese Academy of Sciences, Kunming, 650011, China*
[2] *Department of Astronomy, Cornell University, Ithaca, NY 14853, USA*
[3] *Key Laboratory for the Structure and Evolution of Celestial Objects, Chinese Academy of Sciences, Kunming, 650011, China*

10 April 2015

ABSTRACT

We study the effect of large-scale magnetic fields on the non-axisymmetric inertial-acoustic modes (also called p-modes) trapped in the innermost regions of accretion discs around black holes (BHs). These global modes could provide an explanation for the high-frequency quasi-periodic oscillations (HFQPOs) observed in BH X-ray binaries. There may be observational evidence for the presence of such large-scale magnetic fields in the disks since episodic jets are observed in the same spectral state when HFQPOs are detected. We find that a large-scale poloidal magnetic field can enhance the corotational instability and increase the growth rate of the purely hydrodynamic overstable p-modes. In addition, we show that the frequencies of these overstable p-modes could be further reduced by such magnetic fields, making them agree better with observations.

Key words: accretion, accretion discs - hydrodynamics - waves - black hole - magnetic field

1 INTRODUCTION

Black-hole (BH) X-ray binaries exhibit a wide range of variabilities (e.g. van der Klis 2006; Remillard & McClintock 2006; Yu & Zhang 2013) Of particular interest is the High-Frequency Quasi-Periodic Oscillations (HFQPOs; Remillard & McClintock 2006; Belloni et al. 2012; Belloni & Stella 2014). They have frequencies (several tens to a few hundreds Hz) comparable to the orbital frequency at the Innermost Stable Circular Orbit (ISCO) around the BH (with mass $M \sim 10 M_\odot$) and thus provide a unique probe to study accretion flows near BHs and the effects of strong gravity. These HFQPOs are only observed in the intermediate spectral state of BH X-ray binaries, when the system transitions between the low/hard state (with the X-ray emission dominated by power-law hard photons) and the thermal state (with the emission dominated by thermal disk photons). Interestingly, it is during the intermediate state when episodic jets are observed from the BH X-ray binaries (e.g. Fender et al. 2004). Currently, the physical origin of HFQPOs remains elusive, and a number of ideas and models have been suggested or explored, including the orbital motion of hot spots in the disc (Stella et al. 1999; Schnittman & Bertschinger 2004; Wellons et al. 2014), nonlinear resonances (Abramowicz & Kluzniak 2001; Abramowicz et al. 2007), and oscilla-

tions of finite accretion tori (Rezzolla et al. 2003; Blaes et al. 2006). A large class of models are based on BH discoseismology, in which HFQPOs are identified as global oscillations modes of the inner accretion discs (see Kato 2001, Ortega-Rodriguez et al. 2008 and Lai et al. 2013 for reviews).

In this paper, we study the effect of large-scale magnetic fields on non-axisymmetric ($m > 0$) p-modes [also called inertial-acoustic modes; see Kato (2001) and Wagoner (2008) for reviews] trapped in the innermost region of the accretion disc around a BH. Lai & Tsang (2009) and Tsang & Lai (2009b) showed that these modes, which consist of nearly horizontal oscillations with no vertical structure, can grow in amplitude due to wave absorption at the corotation resonance (where the wave pattern speed ω/m matches the disc rotation rate Ω). This overstability requires that the disc vortensity, $\zeta \equiv \kappa^2/(2\Omega\Sigma)$, where κ is the radial epicyclic frequency and Σ is the surface density (see Horak & Lai 2013 for the full general relativistic version of vortensity), have a positive gradient at the corotation radius r_c (Tsang & Lai 2008; see also Narayan et al. 1987). General relativity (GR) plays an important role: For a Newtonian disc, with $\Omega = \kappa \propto r^{-3/2}$ and a relatively flat $\Sigma(r)$ profile, $d\zeta/dr < 0$, so corotational wave absorption leads to mode damping; with GR, however, κ is non-monotonic in the inner disc (e.g., for a Schwarzschild BH, κ reaches a maximum at $r = 8GM/c^2$ and goes to zero at $r_{\rm isco} = 6GM/c^2$), thus p-modes with frequencies such that $d\zeta/dr > 0$ at r_c are

* Email:cyu@ynao.ac.cn

overstable. Linear calculations based on pseudo-Newtonian potential (Lai & Tsang 2009; Tsang & Lai 2009b) and on full GR (Horak & Lai 2013) show that the mode frequencies approximately agree with the observed HFQPO frequencies (with the BH mass and spin as constrained/measured by observations), although for rapidly rotating BHs, the linear mode frequencies are somewhat too large (Horak & Lai 2013; see below). Nonlinear simulations show that these overstable modes can grow to the large amplitudes and maintain global coherence and well-defined frequencies (Fu & Lai 2013). The mode growth and saturation can also be enhanced by turbulent viscosity (Miranda, Horak & Lai 2015). Overall, these hydrodynamical studies show that non-axisymmetric disc p-modes is a promising candidate to explain HFQPOs in BH X-ray binaries, although a robust diagnostics remains out of reach due to the complexity of the real systems.

Magnetic fields are likely present in BH accretion discs. They may be created as a result of the nonlinear development of the magneto-rotational instability (MRI; Balbus & Hawley 1998). Large-scale poloidal fields may be advected inward with the accretion flow, building up significant strength in the inner disc (e.g., Lubow et al. 1994; Lovelace et al. 2009; Guilet & Ogilvie 2012,2013; Cao & Spruit 2013). Such large-scale fields can lead to production of jets/outflows from accretion discs through the magneto-centrifugal mechanism (e.g., Blandford & Payne 1982). Magnetic fields threading the BH can also lead to relativistic jets from the rotating BHs (McKinney et al. 2012). As noted before, in BH X-ray binaries, episodic jets are observed in the intermediate state, and this is the same state during which HFQPOs are detected. This suggests that to properly study the BH disc oscillation modes, it is necessary to include the effect of large-scale magnetic fields. In our model, the disc and corona (coupled by a large-scale poloidal magnetic field) oscillate together. We suggest that in the intermediate state, large-scale magnetic fields are created (perhaps episodically; cf. Yuan et al. 2009). This would allow the production of episodic jets and the disk oscillations to manifest as HFQPOs in hard X-rays as observed (Remillard & McClintock 2006; Belloni et al. 2012). Tagger and collaborators (Tagger & Pellat 1999; Varniere & Tagger 2002; Tagger & Varniere 2006) have developed a similar picture of disc oscillations, which they termed accretion-ejection instablity, although they focused on the MHD form of Rossby wave instability in the disc (see Lovelace et al. 1999; Yu & Li 2009; Yu & Lai 2013). We note that coherent toroidal magnetic fields in the disc tend to suppress the corotational instability (Fu & Lai 2011). We will focus on poloidal field configurations in this paper.

Recent study by Horak & Lai (2013) provides a full GR corotation instability criterion for disc p-modes. Their full GR results of the mode frequencies are qualitatively in agreement with the pseudo-Newtonian results (Lai & Tsang 2009), but indicate that the theoretical frequencies are too high compared to observations. The discrepancy is most severe for rapidly spinning BHs (such as GRS 1905+105). We show in this paper that including large-scale poloidal fields in the disc may resolve this discrepency.

In our model, we consider fluid perturbations that have no vertical structure inside the disc (i.e., the vertical wavenumber $k_z = 0$). Thus we do not include MRI, which generally involves perturbations with finite k_z. Since the growth of the p-modes is primarily due to in-disc motion, it is adequate to consider 2D disc dynamics. Similar setup has previously been considered by various authors in different contexts (e.g. Spruit et al. 1995; Tagger & Pallet 1999; Lizano et al. 2010).

Our paper is organized as follows. In §2, the basic disc equations with large-scale magnetic fields are derived. In §3, we present the results of p-modes in thin magnetized discs. In §4, we consider the effects of finite disc thickness. and we conclude in §5.

2   BASIC EQUATIONS

We consider a geometrically thin disc and adopt cylindrical coordinate system (r, ϕ, z). We use the the pseudo-Newtonian potential of Paczynski & Wiita (1980)

$$\Phi = -\frac{GM}{r - r_s} , \qquad (1)$$

where $r_s = 2GM/c^2$ is the Schwarzschild radius. For this potential, the free particle (Keplerian) orbital frequency is

$$\Omega_K = \sqrt{\frac{GM}{r}} \frac{1}{r - r_s}, \qquad (2)$$

and the radial epicyclic frequency κ is given by

$$\kappa = \Omega_K \sqrt{\frac{r - 3r_s}{r - r_s}}. \qquad (3)$$

The innermost stable circular orbit (ISCO), defined by $\kappa^2 = 0$, is located at $r_{\rm isco} = 3r_s$. The epicyclic frequency reaches a peak at $r_{\rm max} = (2 + \sqrt{3})r_s$. Note that the GR effect plays an essential role in the corotational instability of $p-$modes. In Newtonian theory, $\kappa = \Omega \propto r^{-3/2}$, so $d\zeta/dr < 0$ if the surface density Σ is constant; with GR, $d\zeta/dr > 0$ for $r < r_{\rm max}$.

When large-scale magnetic fields thread the thin conducting disc, the height-integrated mass continuity equation and momentum equation read

$$\frac{\partial \Sigma}{\partial t} + \nabla_\perp \cdot (\Sigma \mathbf{u}) = 0, \qquad (4)$$

$$\frac{d\mathbf{u}}{dt} = -\frac{1}{\Sigma}\nabla_\perp P + \frac{1}{4\pi\Sigma} B_z [\mathbf{B}]_-^+ + \mathbf{g}, \qquad (5)$$

where $\nabla_\perp$ is 2D operator acting on the disc plane, Σ, P and $\mathbf{u}$ are the surface density, height-integrated pressure and height-averaged velocity, respectively, $\mathbf{g} = -g(r)\hat{r}$, with $g = GM/(r - r_s)^2$, is the gravitational acceleration, $[\mathbf{B}]_-^+ \equiv \mathbf{B}(z = H) - \mathbf{B}(z = -H)$ (with H the half-thickness of the disc), and we have used $[B^2]_-^+ = 0$. The effect of finite disc thickness will be considered in Section 4.

The unperturbed velocity of an equilibrium disc is $\mathbf{u} = (0, r\Omega, 0)$ (in cylindrical coordinates), with the angular velocity given by

$$-\Omega^2 r = -\frac{1}{\Sigma}\frac{dP}{dr} - \frac{d\Phi}{dr} + \frac{B_z}{2\pi\Sigma}B_r^+, \qquad (6)$$

where $B_r^+ = B_r(z = H) = -B_r^-$. The unperturbed disc has $B_\phi^+ = 0$. Note that B_r is nonzero only outside the discs, which has different signs above and below the disc. Inside the disk, B_r is zero (so that the differential rotation of the disc would not lead to generation of B_ϕ inside the disc). **It should be mentioned that the field configuration**

adopted in this paper is highly idealized. **A magneto-centrifugal disc wind or jet, if present, will certainly involve B_ϕ in the background state. For simplicity, we assume that the magnetic field outside the disc to be a potential field.** The disc surface density is assumed to have a power law form $\Sigma \propto r^{-p}$, where p is the density index. **We also try various behavior of the surface density and the magnetic field, in which the profile of B_z/Σ can be increasing, decreasing, or constant. We find that the results are qualitatively similar. Without loss of generality, we fix $p = 1$ throughout this paper.**

The dynamics of the disc is coupled with the large scale poloidal magnetic field outside the disc, i.e., the disc magnetosphere. We now consider small-amplitude perturbations of the disc. We assume that all perturbed quantities have the dependence $\exp(im\phi - i\omega t)$, where $m = 1, 2, \cdots$ is the azimuthal wave number and ω is the complex frequency. Then the linearized fluid perturbation equations become

$$-i\tilde{\omega}\,\delta\Sigma = -\nabla_\perp \cdot (\Sigma\,\delta\mathbf{u})\,, \tag{7}$$

$$-i\tilde{\omega}\,\delta u_r - 2\Omega\,\delta u_\phi = -\frac{\partial}{\partial r}\,\delta h + \frac{B_z}{2\pi\Sigma}\,\delta B_r^+ \\ + \frac{B_r^+}{2\pi}\delta\left(\frac{B_z}{\Sigma}\right), \tag{8}$$

$$-i\tilde{\omega}\,\delta u_\phi + \frac{\kappa^2}{2\Omega}\,\delta u_r = -\frac{im}{r}\,\delta h + \frac{B_z}{2\pi\Sigma}\,\delta B_\phi^+\,, \tag{9}$$

where $\tilde{\omega} = \omega - m\Omega$ is the wave frequency in the rotating frame of the fluid, and $\delta h = \delta P/\Sigma$ is the enthalpy perturbation (we assume barotropic discs). The magnetic field induction equation in the disc reads

$$-i\tilde{\omega}\,\delta B_z = -\nabla_\perp \cdot (B_z\,\delta\mathbf{u})\,. \tag{10}$$

Combining Eqs. (7) and (10), we have

$$\delta\left(\frac{B_z}{\Sigma}\right) = -\xi_r\frac{d}{dr}\left(\frac{B_z}{\Sigma}\right), \tag{11}$$

where $\xi_r = \delta u_r/(-i\tilde{\omega})$ is the Lagrangian displacement. Equation (11) can also be derived from $(d/dt)(B_z/\Sigma) = 0$. In terms of ξ_r and δh, the magnetic field perturbation is

$$\delta B_z = D_1\xi_r + D_2\delta h, \tag{12}$$

with

$$D_1 = B_z\frac{d}{dr}\left(\ln\frac{\Sigma}{B_z}\right), \quad D_2 = \frac{B_z}{c_s^2}, \tag{13}$$

where c_s is the disc sound speed.

To determine δB_r^+ and δB_ϕ^+, we assume that the magnetic field outside the disc is a potential field (see Spruit et al. 1995; Tagger & Pallet 1999). This is equivalent to assuming that the Alfven speed above and below the disc is sufficiently high that currents are dissipated rapidly (on the disc dynamical timescale). Define the "magnetic potential" $\delta\Phi_M$ outside the disc via

$$\delta\mathbf{B} = -\text{sign}(z)\nabla\delta\Phi_M. \tag{14}$$

Then $\delta\Phi_M$ satisfies the Poisson equation (Tagger & Pallet 1999)

$$\nabla^2\delta\Phi_M = -2\,\delta B_z\,\delta(z), \tag{15}$$

where $\delta(z)$ is the Dirac delta function. The integral solution of (15) is

$$\delta\Phi_M(r) = \int\delta B_z(r')\left[\frac{\alpha}{2}\,b_{1/2}^m(\alpha)\right]dr', \tag{16}$$

where $\alpha = r'/r$, and the Laplace coefficient is defined by

$$b_s^m(\alpha) = \frac{2}{\pi}\int_0^\pi\frac{\cos m\phi}{(\alpha^2 + \epsilon_0^2 + 1 - 2\alpha\cos\phi)^s}\,d\phi, \tag{17}$$

with ϵ_0 the softening parameter (of order the disc aspect ratio H/r). The perturbed radial magnetic field at the upper disc surface is

$$\delta B_r^+ = -\frac{d}{dr}\delta\Phi_M \\ = \int\delta B_z(r')\left(\frac{\alpha}{2r}\right)\left[b_{1/2}^m(\alpha) + \alpha\frac{db_{1/2}^m(\alpha)}{d\alpha}\right]dr', \tag{18}$$

and the azimuthal field is $\delta B_\phi^+ = -(im/r)\delta\Phi_M$.

In our numerical calculations, we use ξ_r and δh as the basic variables. The perturbation equations are

$$\frac{d\xi_r}{dr} = -\left(\frac{2m\Omega}{r\tilde{\omega}} + \frac{1}{r} + \frac{d\ln\Sigma}{dr}\right)\xi_r \\ -\left(\frac{1}{c_s^2} - \frac{m^2}{r^2\tilde{\omega}^2}\right)\delta h + \frac{m^2}{r^2\tilde{\omega}^2}\frac{B_z}{2\pi\Sigma}\,\delta\Phi_M, \tag{19}$$

$$\frac{d}{dr}\delta h = \left(\tilde{\omega}^2 - \kappa^2 + \frac{B_r^+}{2\pi\Sigma}D_1\right)\xi_r + \frac{2m\Omega}{r\tilde{\omega}}\,\delta h \\ -\frac{B_z}{2\pi\Sigma}\frac{d\delta\Phi_M}{dr} + \frac{2m\Omega}{r\tilde{\omega}}\frac{B_z}{2\pi\Sigma}\,\delta\Phi_M. \tag{20}$$

To obtain global trapped modes, wave reflection must occur at the inner disc boundary $r_{\rm in}$. To focus on the effect of corotational instability, we adopt a simple inner boundary condition, i.e., the radial velocity perturbation vanishes at the inner boundary, $\delta u_r = 0$. **This implies a reflecting inner disc edge, for example due to the presence of a magnetosphere around the black hole (e.g., Bisnovatyi-Kogan & Ruzmaikin 1974, 1976; Igumenshchev et al. 2003; Rothstein & Lovelace 2008; McKinney et al. 2012; see Tsang & Lai 2009a and Fu & Lai 2012 for more detailed treatment of the magnetosphere-disc interface oscillations).** As we are interested in the self-excited modes in the inner region of the disc, we implement the radiative outer boundary conditions such that waves propagate away from the disc (e.g., Yu & Li 2009). The ordinary equations (19) and (20), together with the two boundary conditions at the inner and outer disk edge, form an eigenvalue problem. Since the eigenfrequency ω is in general complex, equations (19)-(20) are a pair of first-order differential equations with complex coefficients which are functions of r. We solve these equations using the relaxation method (Press et al. 1992), replacing the ODEs by finite-difference equations on a mesh of points covering the domain of interest (typically $r_{\rm isco} < r < 2.5r_{\rm isco}$). According to Eqs. (12), (16) and (18), both the magnetic potential and its derivative can be expressed in terms of the linear combination of ξ_r and δh. For numerical convenience, we calculate the terms in the square bracket in Eqs. (16) and (18) and store them for later use. Note that these terms are computed only once and can be used repetitively. The wave equations (19) and (20) can be cast in a matrix form that only deals with the variables $d\xi_r$ and dh. Standard relaxation scheme can be applied to the resulting matrix.
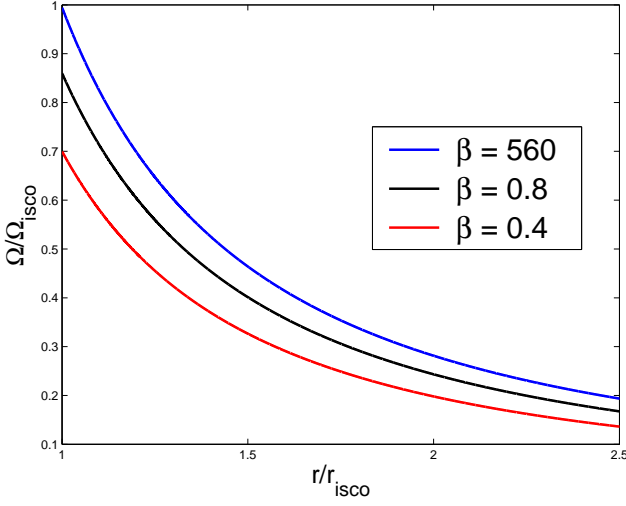
Figure 1. Rotation curve for different value of β when $B_r^+ = B_z$. With the increase of magnetic stress, the angular velocity is reduced.

We use uniform grid points in our calculations. The grid point number is typically chosen to be 350. The relaxation method requires an initial trial solution that is improved by the Newton–Raphson scheme. After iterations the initial trial solution converges to the eigenfunction of the the two-point boundary eigenvalue problem.

3   RESULTS FOR THIN DISCS

For our numerical calculations, we adopt the disc sound speed $c_s = 0.1(r\Omega_K)$. The magnitude of B_z is specified by the dimensionless ratio

$$\hat{B}_z = \frac{B_z}{(\Sigma_0 \Omega_0^2 r_0)^{1/2}}, \tag{21}$$

where the subscript "0" implies that the quantities evaluated at $r = r_{\rm isco}$. The corresponding plasma β parameter in the disc at $r = r_{\rm isco}$ is

$$\beta_0 = \frac{8\pi\rho c_s^2}{B_z^2}\bigg|_{r=r_{\rm isco}} = \frac{4\pi H_0}{r_0}\hat{B}_{z0}^{-2}, \tag{22}$$

where we have used $H = c_s/\Omega_K \simeq c_s/\Omega$. The magnetic field is chosen such the plasma β is equal to β_0 at $r = r_{\rm isco}$ throughout the disc. Note that magnetic field B_z in the disc varies approximately as $B_z \propto r^{-1-p/2}$, where p is the surface density power law index. We solve for the equilibrium rotation profile using Eq. (6). **Note that when $B_r^+ = 0$, the rotation profile of the disc is unaffected by B_z. When $B_r^+ = B_z$, the equilibrium rotation profile of the disc is changed from the nonmagnetic disc. In Fig. 1 we show the rotation curve in the case of $B_r^+ = B_z$ for different value of β. We clearly see the reduction in the angular velocity of the equilibrium disc due to the outward $B_z B_r^+$ stress on the disc.**

The upper panel of Figure 2 shows the growth rate of the p-modes for different magnetic field strengths. When $B_r^+ = 0$, we see that with the increase of magnetic field, the p-mode growth rate varies in a non-monotonic way. The growth rate first increases and then decreases. At $\beta \sim 0.5$,
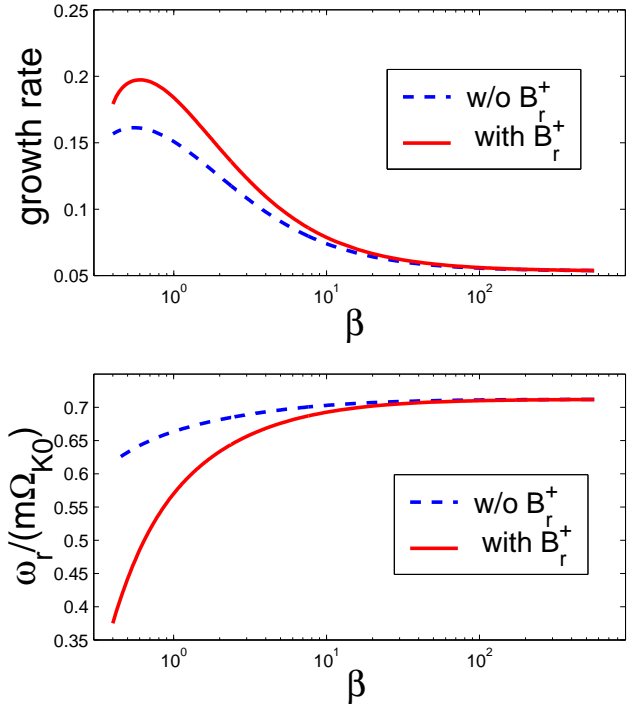

Figure 2. The growth rate (in units of $\Omega_{K0} = \Omega_{\rm isco}$) (upper panel) and the real frequency (lower panel) of the $m = 2$ p-mode as a function of the plasma β parameter for thin discs [with the corresponding vertical magnetic field strength B_z given by Eq. (22)]. The blue dashed line is the case of $B_r^+ = 0$, and the red solid line $B_r^+ = B_z$.
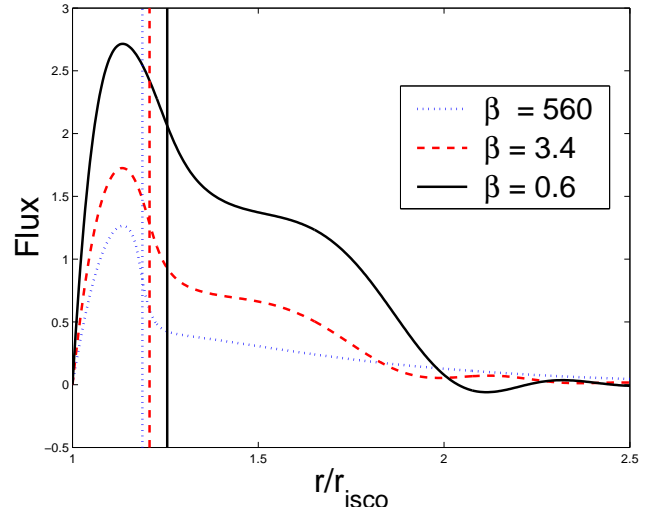

Figure 4. The angular momentum flux associated with the p-mode in disc with $\hat{B}_r^+ = 0$. The blue dotted line is for the weakly magnetized disc ($\beta \sim 600$), and the red dashed line and black solid line are for more strongly magnetized disc ($\beta = 3.4$ and 0.6). In all cases, the eigenfunction is normalized so that the maximum velocity perturbation, δu_r, equals unity. The higher angular momentum flux for the more strongly magnetized case is consistent with the larger mode growth rate. **The vertical lines denote the corotation resonances, which are located at $r_c = 1.19, 1.21, 1.26$, respectively.**
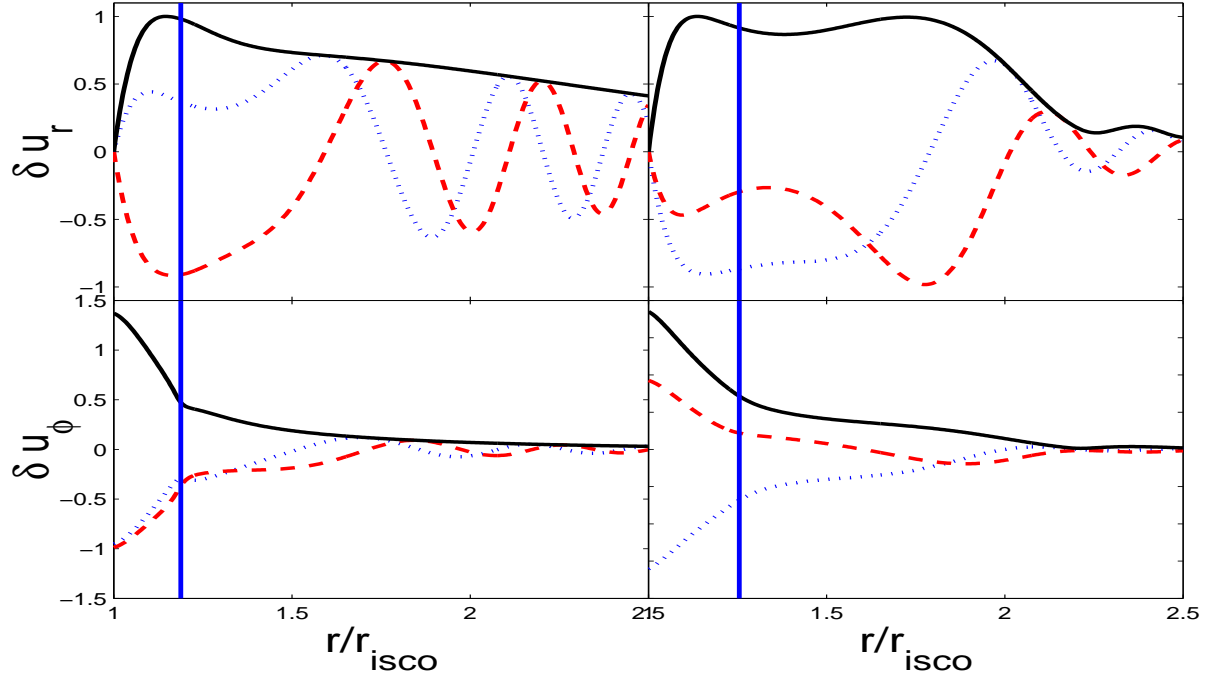
Figure 3. Eigenfunctions of the $m = 2$ the p-modes trapped in the inner most region in the disc. The left panels show the weakly magnetized case ($\beta \sim 600$); the difference with the nonmagnetic case is essentially indistinguishable. The right panels have $\beta \sim 0.6$ (strongly magnetized). The top panels show δu_r (the dotted line is for the real part, the dashed line the imaginary part, and the solid line the absolute value), and the bottom panels show δu_ϕ. **The corotation resonances are marked by the vertical lines, which are located at $r_c = 1.19, 1.26$, respectively.**

the growth rate is enhanced by a factor of 3 compared to the $B_z = 0$ value. When $B_r^+ = B_z$, the overall behavior of the growth rate is similar to the case of $B_r^+ = 0$, but the maximum growth rate is about 30% higher than disc with $B_r^+ = 0$. The mode frequencies are shown in the lower panel in Fig. 2. For the disc with $B_r^+ = 0$, the mode frequency decreases monotonically from $\omega_r \simeq 0.7m\Omega_{K0}$ to $\omega_r \simeq 0.6m\Omega_{K0}$ with the increase of magnetic field. For disc with $B_r^+ = B_z$, the frequency can be reduced by a factor about 2, changing from $\omega_r \simeq 0.7m\Omega_{K0}$ to $\omega_r \simeq 0.35m\Omega_{K0}$.

Figure 3 gives some examples of the $m = 2$ eigenfunctions of p-modes trapped in the innermost region of the disc. The left panels show the case with very weak magnetic fields, and the the right panels show the magnetized case with $\hat{B}_r^+ = \hat{B}_z = 0.78$. The amplitudes of the eigenfunctions are normalized so that the maximum absolute value of the radial velocity perturbation $|\delta u_r|$ equals unity (this maximum occurs at $r \simeq r_0$).

To understand the origin of the enhanced p-mode growth rate for magnetized discs, we show in Fig. 4 the angular momentum flux associated with the eigenmode for the weakly magnetized disc (plasma $\beta \sim 600$) and for the more strongly magnetized discs (plasma $\beta = 3.4$ and 0.6). The angular momentum flux $F(r)$ across a cylinder of radius r is given by (e.g., Goldreich & Tremaine 1979)

$$F(r) = \left\langle r^2 \int_0^{2\pi} \Sigma \delta u_r \delta u_\phi d\phi \right\rangle = \pi \Sigma r^2 \Re \left(\delta u_r \delta u_\phi^* \right) \quad (23)$$

where $\langle \rangle$ designates time average and the superscript $*$ denotes complex conjugate. Note that waves carry negative (positive) angular momentum inside (outside) the corota-

tion. The net positive (outward) angular momentum flux $F(r)$ around the corotation indicates the growth of the p-modes. Higher angular momentum fluxes imply higher instability growth rates (see Fig. 4).

4 EFFECTS OF FINITE DISC THICKNESS

4.1 Model Equations

When finite thickness of the disc is considered, an "internal" magnetic force term should be added to the right-hand side of Eq. (5):

$$\mathbf{f} = \frac{1}{\Sigma} \int dz \left[-\nabla_\perp \left(\frac{B^2}{8\pi} \right) + \frac{1}{4\pi} \left(\mathbf{B} \cdot \nabla_\perp \right) \mathbf{B} \right]. \quad (24)$$

Obviously, to include the 3D effect rigorously would require examining the vertical stratification of the density and magnetic field inside the disc – this is beyond the scope of this paper. Here we consider a simple model where the internal density of the disc is assumed to be independent of z, so that

$$\Sigma = 2\rho H, \quad P = 2pH. \quad (25)$$

Then the internal magnetic force simplifies to

$$\mathbf{f} = \frac{1}{4\pi\rho} \left[-\nabla_\perp \left(\frac{B^2}{2} \right) + \left(\mathbf{B} \cdot \nabla_\perp \right) \mathbf{B} \right]. \quad (26)$$

We assume that only vertical magnetic field exists inside the unperturbed disc. The equilibrium rotational profile is then

determined by

$$-\Omega^2 r = -\frac{1}{\Sigma}\frac{dP}{dr} - g + \frac{B_z}{2\pi\Sigma}B_r^+ - \frac{B_z}{2\pi\Sigma}\left(H\frac{dB_z}{dr}\right) \ . \quad (27)$$

To derive the modified perturbation equations including $\delta\mathbf{f}$, it is convenient to define a new perturbation variable $\delta\Pi$ in place of δh:

$$\delta\Pi \equiv \frac{\delta P}{\Sigma} + \frac{B_z\delta B_z}{4\pi\rho} = c_s^2\frac{\delta\rho}{\rho} + \frac{B_z\delta B_z}{4\pi\rho}. \quad (28)$$

After some algebra, the final disc perturbation equations can be written in the following form:

$$\frac{d\xi_r}{dr} = -\left(\frac{2m\Omega}{r\tilde\omega} + \frac{1}{r} + \frac{d\ln\Sigma}{dr} + D_4\right)\xi_r$$
$$+ \left(\frac{m^2}{r^2\tilde\omega^2} - D_5\right)\delta\Pi + \frac{m^2}{r^2\tilde\omega^2}\frac{B_z}{2\pi\Sigma}\delta\Phi_M, \quad (29)$$

$$\frac{d}{dr}\delta\Pi = \left(\tilde\omega^2 - \kappa^2 + \frac{B_r^+}{2\pi\Sigma}D_3 + D_6\right)\xi_r$$
$$+ \left(\frac{2m\Omega}{r\tilde\omega} + D_7 - \frac{d\ln\rho}{dr}\right)\delta\Pi$$
$$+ \frac{2m\Omega}{r\tilde\omega}\frac{B_z}{2\pi\Sigma}\delta\Phi_M - \frac{B_z}{2\pi\Sigma}\frac{d\delta\Phi_M}{dr}, \quad (30)$$

where $D_3 = D_1$, and

$$D_4 = \frac{-c_a^2}{c_s^2 + c_a^2}\frac{d}{dr}\left(\ln\frac{\Sigma}{B_z}\right), \quad c_a^2 = \frac{B_z^2}{4\pi\rho}, \quad (31)$$

$$D_5 = \frac{1}{c_s^2 + c_a^2}, \quad (32)$$

$$D_6 = \left[\frac{1}{\rho}\frac{d(p + \frac{1}{8\pi}B_z^2)}{dr}\right]D_4, \quad (33)$$

$$D_7 = \left[\frac{1}{\rho}\frac{d(p + \frac{1}{8\pi}B_z^2)}{dr}\right]D_5. \quad (34)$$

4.2 Results

Finite disc thickness has two-fold effects on the p-mode corotation instability : the first is the change in the equilibrium rotation profile and the second is the direct effect of $\delta\mathbf{f}$. With these two effects included, we calculate the eigenmodes of the disc using the same method as in Section 3. The results are shown in Figure 5. The red solid line shows the case with $B_r^+ = B_z$ and the blue dashed line shows the case with $B_r^+ = 0$. We find that for the parameter considered ($c_s = 0.1r\Omega_K$, or $H/r = 0.1$), the p-mode growth rate is decreased compared to the $H/r \to 0$ limit. More specifically, the maximum growth rate is about $25\% - 30\%$ lower. However for sufficiently strongly-magnetized disc (plasma $\beta \sim 0.4$), especially for disc with radial magnetic field in the magnetosphere, the oscillation frequency of the overstable mode can be reduced further, changing from $\omega_r \simeq 0.7m\Omega_{K0}$ to $\omega_r \simeq 0.2m\Omega_{K0}$, which is reduced by about of factor 3 compared to the pure hydrodynamic mode.

As noted in Section 1, full GR calculations of hydrodynamic disc p-modes show that, for accretion discs around extreme Kerr BHs, the oscillation frequency is close to $m\Omega_{K0}$ (Horak & Lai 2013). However, observations reveal that the frequencies of HFQPOs are usually smaller than this value by a factor of 2-3. This discrepancy indicates that pure hydrodynamic disc p-modes without magnetic field can not
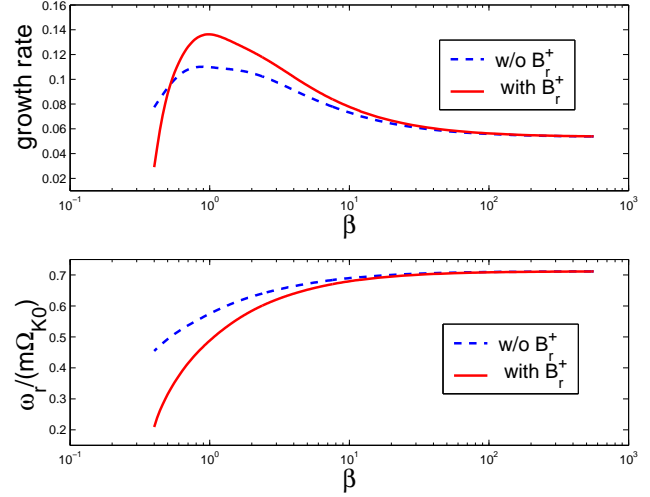

Figure 5. Growth rate (in units of $\Omega_{K0} = \Omega_{\mathrm{isco}}$) and frequency of the unstable $m = 2$ p-mode as a function of the plasma β parameter for discs with finite thickness. The blue dashed line is for the case with $B_r^+ = 0$, while the red solid line for the case of $B_r^+ = B_z$.

explain HFQPOs in X-ray binaries, particularly for high-spin sources (such as GRS 1905+105). When the large-scale poloidal magnetic field is included, this discrepancy can be resolved since the reduction in oscillation frequency makes the theoretical p-mode prediction more consistent with the observed values.

In addition, we find that the first effect, i.e., the change of the equilibrium disc rotation profile **induced by the disk finite thickness**, plays a minor role in the disc p-mode instability. To make this point more clearly, we artificially discard the last term on the right hand side of Equation (27). We find that results are very close to those with this term included (the detailed results are not shown in Fig. 5, since they are very close to the curves in Fig. 5).

5 DISCUSSION AND CONCLUSION

In this paper we have carried out linear analysis of p-modes in BH accretion discs threaded by large-scale magnetic fields. These modes reside in the innermost region in the disc, can become overstable driven by corotational instability, and may be responsible for the observed high-frequency quasi-periodic oscillations (HFQPOs) in BH X-ray binaries. Our results show that the large-scale magnetic field can increase the mode growth rates significantly (by a factor of a few for plasma $\beta \sim 1$ in the disc). It can also reduce the mode frequencies, bringing the theoretical values into agreement with the observed HFQPO frequencies.

It is important to note that since episodic jets are observed in the intermediate state of BH X-ray binaries when HFQPOs are detected, a proper treatment of large-scale magnetic fields is crucial for understanding the disc-jet-QPO connections in accreting BH systems (e.g. Fender et al. 2004). Although our treatment of the disc magnetic fields is somewhat idealized (e.g., toroidal fields, vertical stratification and MRI turbulence are not included), it demonstrates

the importance of including magnetic fields in studying BH disc oscillations and confronting with observations.

Overall, our study shows that global oscillations of BH accretion discs, combining the effects of general relativity and magnetic fields, is a promising candidate for understanding HFQPOs observed in BH X-ray binaries and similar oscillations potentially observed in intermediate and supermassive BHs (e.g., Pasham, Strohmayer & Mushotzky 2014). Important caveats and uncertainties (see Lai et al. 2013 for a concise review of various issues) remain in our treatment of the physical condition of the innermost accretion flows around BHs (e.g., the BH magnetosphere - disc interface; see Tsang & Lai 2009a; Fu & Lai 2012; Miranda et al. 2015). It is hoped that future observations with more sensitive X-ray timing telescopes (such as LOFT, see Feroci et al. 2014) will shed more light on the origin of variabilities of accreting BHs (e.g. Belloni & Stella 2014).

REFERENCES

Abramowicz M. A., Kluzniak W., 2001, A&A, 374, L19
Abramowicz M. A., et al. 2007, RMxAA, 27, 8
Balbus S. A., & Hawley J. F., 1998, Rev. Mod. Phys., 70, 1
Belloni T. M., Sanna A., Mendez M., 2012, MNRAS, 426, 1701
Belloni, T.M., Stella, L. 2014, Space Sci. Rev., 183, 43 (arXiv:1407.7373)
Bisnovatyi-Kogan, G.S., Ruzmaikin, A. A., 1974, Ap&SS, 28, 45
Bisnovatyi-Kogan, G.S., Ruzmaikin, A. A., 1976, Ap&SS, 42, 401
Blaes O. M., Arras P., Fragile P. C., 2006, MNRAS, 369, 1235
Blandford, R. D., & Payne, D. G. 1982, MNRAS, 199, 883
Cao, X., Spruit, H.C. 2013, ApJ, 765, 149
Fender, R.P., Belloni, T.M., Gallo, E. 2004, MNRAS, 355, 1105
Feroci, M., et al. 2014, arXiv:1408.6526
Fu W., & Lai D., 2011, MNRAS, 410, 399
Fu, W., & Lai, D., 2012, MNRAS, 423, 831
Fu, W., & Lai, D., 2013, MNRAS, 431, 3697
Goldreich, P., & Tremaine, S. 1979, ApJ, 233, 857
Guilet, J., Ogilvie, G.I. 2012, MNRAS, 424, 2097
Guilet, J., Ogilvie, G.I. 2013, MNRAS, 430, 822
Horák, J., Lai, D., 2013, MNRAS, 434, 2761
Igumenshchev, I.V., Narayan, R., Abramowicz, M.A., 2003, ApJ, 592, 1042
Kato, S. 2001, PASJ, 53, 1
Lai, D., Fu, W., Tsang, D., Horak, J., & Yu, C. 2013, IAU Symposium, 290, 57 (arXiv:1212.5323)
Lai D., & Tsang D., 2009, MNRAS, 393, 979
Lizano S., et al., 2010, ApJ, 724, 1561
Lovelace, R. V. E.; Li, H.; Colgate, S. A.; Nelson, A. F., 1999, 513, 815
Lovelace, R.V.E., Rothstein, D.M., Bisnovatyi-Kogan, G. 2009, ApJ, 701, 885
Lubow, S. H., Papaloizou, J. C. B., & Pringle, J. E. 1994, MNRAS, 267, 235
McKinney J. C., Tchekhovskoy A., Blandford R. D., 2012, MNRAS, 423, 3083
Miranda, R., Hirak, J., Lai, D. 2015, MNRAS, 446, 240
Narayan R., Goldreich P., & Goodman J., 1987, MNRAS, 228, 1
Ortega-Rodríguez, M., Silbergleit, A., Wagoner, R., 2008, GApF D, 102, 75
Paczynsky B., & Wiita P. J., 1980, A&A, 88, 23
Pasham, D. R., Strohmayer, T. E., & Mushotzky, R. F. 2014, Nature, 513, 74
Press W. H., Teukolsky S. A., Vetterling W. T., Flannery B. P., 1992, Numerical Recipes in FORTRAN. Cambridge Univ. Press, Cambridge
Remillard R. A., McClintock J. E., 2006, ARA&A, 44, 49
Rezzolla L., Yoshida S., Maccarone T. J., Zanotti O., 2003, MNRAS, 344, L37
Rothstein, D. M., Lovelace, R. V. E., 2008, ApJ, 677, 1221
Schnittman J. D., & Bertschinger, E., 2004, ApJ, 606, 1098
Spruit H. C., Stehle R., & Papaloizou J. C. B., 1995, MNRAS, 275, 1223
Stella L., Vietri M., Morsink S. M. 1999, ApJ, 524, L63
Tagger M., & Pellet R., 1999, A&A, 349, 1003
Tagger M., Varniere P. 2006, ApJ, 652, 1457
Tsang, D., & Lai, D., 2008, MNRAS, 387, 446
Tsang, D., & Lai, D., 2009a, MNRAS, 396, 589
Tsang, D., & Lai, D., 2009b, MNRAS, 400, 470
van der Klis M., 2006, in Lewin W. H. G., van der Kils M., eds, Compact Stellar X-ray sources. Cambridge Univ. Press, Cambridge
Varniere, P., & Tagger, M., 2002, A&A, 394, 329
Wagoner R. V., 2008, J. Phys: Conf. Series, Vol.118, 012006
Wellons S., Zhu Y.; Psaltis, D., Narayan R., & McClintock J. E., 2014, ApJ, 785, 142
Yu C., & Li H., 2009, ApJ, 702, 75
Yu C. & Lai D., 2013, MNRAS, 429, 2748
Yu, W., & Zhang, W. 2013, ApJ, 770, 135
Yuan, F., Lin, J., Wu, K., & Ho, L.C. 2009, MNRAS, 395, 2183